

The effect of microstructure on the mechanical behavior and fracture mechanism in a 7050-T76 aluminum alloy

O. E. Alarcon

LABMAT-EMC/CTC/UFSC, Florianopolis, SC (Brazil)

A. M. M. Nazar

DEMA-UNICAMP, Campinas, SP (Brazil)

W. A. Monteiro

DM-CNEN/IPEN, Sao Paulo, SP (Brazil)

(Received August 28, 1990; in revised form November 13, 1990)

Abstract

The mechanical behavior of the 7050 aluminum alloy with partially recrystallized (PR), recrystallized (R) and unrecrystallized (UR) microstructures was investigated. The UR and R microstructures were produced by thermomechanical treatment. The monotonic tensile properties showed no significant difference between the microstructures, but the fracture toughness of the UR microstructure showed a significant improvement over that of the PR and R microstructures. The higher fracture toughness was associated with a transgranular fracture mode and larger blunting of the crack tip. *In situ* deformation studies by transmission electron microscopy showed that the fracture process was due to a stress concentration effect at the crack tip.

1. Introduction

Investigations initiated about 20 years ago, on the metallurgical parameters affecting fracture toughness [1–8] and developments in fracture mechanical testing [9], provided basic information leading to the development of high strength aluminum alloy with significant improvements in fracture toughness. The relevant metallurgical factors are related to [1]: (a) the distribution and resistance of particles to cleavage and decohesion; (b) the local strain concentration and precipitate-free zones; (c) the grain size and morphology.

Starke and Lin's [4] investigations have shown that the deformation process responsible for the fracture mechanism of aluminum alloy can be summarized as follows. For ageing conditions that do not produce precipitate-free zones, deformation occurs within the grain, and the coherent and partially coherent precipitates are sheared by moving dislocations resulting in coarse planar slip bands and strain localization. Crack nucleation occurs at slip grain boundary intersections and subsequent propagation follows the slip bands or grain boundaries. In contrast, the plastic defor-

mation is located in soft regions if the ageing conditions produce precipitate-free zones. In this case the cracks nucleate at a grain boundary triple junction or at grain boundary precipitates and propagate intergranularly within the zones. Very large recrystallized grains present in commercial 7XXX aluminum alloys, with a partially recrystallized (PR) microstructure, can also be associated with intergranular fracture due to strain concentration in grain boundaries [4, 5, 8]. The changes in morphology and reduction in grain size produced by thermomechanical treatments (TMTs) [4–7] have been shown to be effective in preventing premature fracture by reducing the dislocation pile-up length, which concentrates strain in the grain boundaries.

The main purpose of this investigation was to study the influence of grain structure, as produced by TMTs, on the mechanical behavior and fracture mechanism in a 7050 T76 aluminum alloy.

2. Experimental procedures

The commercial 7050 aluminum alloy used in this study was a rolled plate 38 mm thick with a

PR microstructure [10] (see Fig. 5(a) below) made by Alcoa-U.S.A. and supplied by Embraer-Brasil. The nominal chemical composition was [11]: 2.23% Cu; 2.25% Mg; 6.20% Zn; 0.12% Zr; less than 0.12% Fe; less than 0.15% Si. Some as-received material was homogenized (480 °C for 24 h) and processed by TMTs according to the schedules given in Fig. 1.

Samples were taken for each TMT step to study the microstructural behavior by transmission electron microscopy (TEM). The microstructural parameters related to grain size and distribution of inclusions were studied using optical microscopy, a granulometric analyzer (TGZ-Zeiss) and metallographic quantitative methods [12, 13]. The hardening precipitate distribution and the slip behavior were characterized using TEM on thin foil samples previously prepared by electropolishing in a Tenupol using a solution of three parts methanol to one part nitric acid cooled to -20 °C.

The tensile samples of 3 mm thickness were machined so that the loading axis was parallel to the rolling direction according to ASTM E 8M-1985. The fracture toughness was characterized using the crack opening displacement (COD) test according to BS 5762 for a three-point bend specimen taken from the L-T and T-L directions according to ASTM E 399. The maximum load criterion [14] was utilized for determining the fracture toughness CTOD. The fracture surfaces of samples from both types of test were analyzed using scanning electron microscopy (SEM). Some tensile samples were strengthened at 2% elongation to study the slip behavior in TEM. Other thin foil samples were also prepared to investigate the deformation and fracture mechanisms using *in situ* observation of deformation by TEM (200 kV). In this case a lithographical method using a photoresister and subsequent corrosion in orthophosphoric and nitric acid was utilized for sample preparation [10-14]. This method does not introduce strain during sample preparation.

3. Results and discussion

3.1. TMTs and microstructure

The TMT shown schematically in Fig. 1(a) was used to produce a fine recrystallized grain microstructure (R) in the 7050 aluminum alloy. The process, as selected, increases the volumetric fraction of coarse particles during preageing and consequently increases the tendency towards an

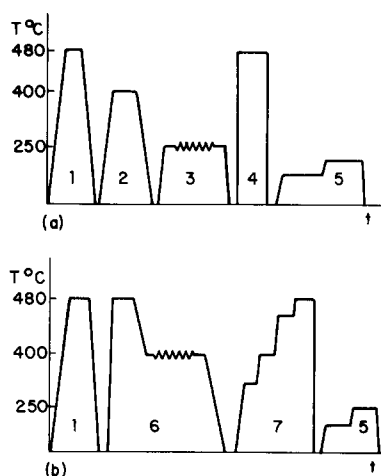


Fig. 1. TMTs selected to produce (a) R and (b) UR microstructures: 1, solution heat treatment (480 °C for 30 min); 2, ageing treatment (400 °C for 8 h); 3, rolling deformation (80% thickness reduction at 250 °C); 4, solution heat treatment (480 °C for 30 min, with a 4 °C s⁻¹ heating rate); 5, final ageing T76 condition (120 °C for 5 h plus 163 °C for 13 h (± 1 °C)); 6, solution heat treatment (480 °C for 1 h, followed by 87% thickness reduction by rolling at 400 °C); 7, solution heat treatment (480 °C for 30 min, with a 1 °C min⁻¹ heating rate and 30 min steps at 350, 400 and 450 °C).

inhomogeneous strain distribution during the subsequent work operation, which enhances the possibility of recrystallization during heat treatment [10, 14, 15]. The time and temperature parameters for the preageing treatment have been selected according to results obtained by Wert *et al.* [16, 17]. This treatment produced a bimodal particle distribution; equilibrium precipitates, with approximately 50 nm diameter and 0.034 volumetric fraction and containing T phases (Mg₃Zn₃Al₂) [18], showed an irregular morphology, with 0.5-1.5 μm length and 0.2-0.5 μm width (Fig. 2(a) and Fig. 2(b) respectively). The matrix deformation substructure showed a well-defined elongated subgrain distribution characteristic of heavily worked and recovered aluminum alloy [19, 20]. The subgrain size was typically around 0.5 μm in the short transverse direction and 1-2 μm in the longitudinal direction (Fig. 2(c)). However, a very different deformation distribution was observed around the coarse particles. Strong deformation zones were formed around these particles as shown in Fig. 2(d). These zones contained groups of smaller subgrains with similar orientation and higher density of dislocations inside the subgrains. The nucleation of recrystallization occurs probably around the coarse particles due to a polygoniza-

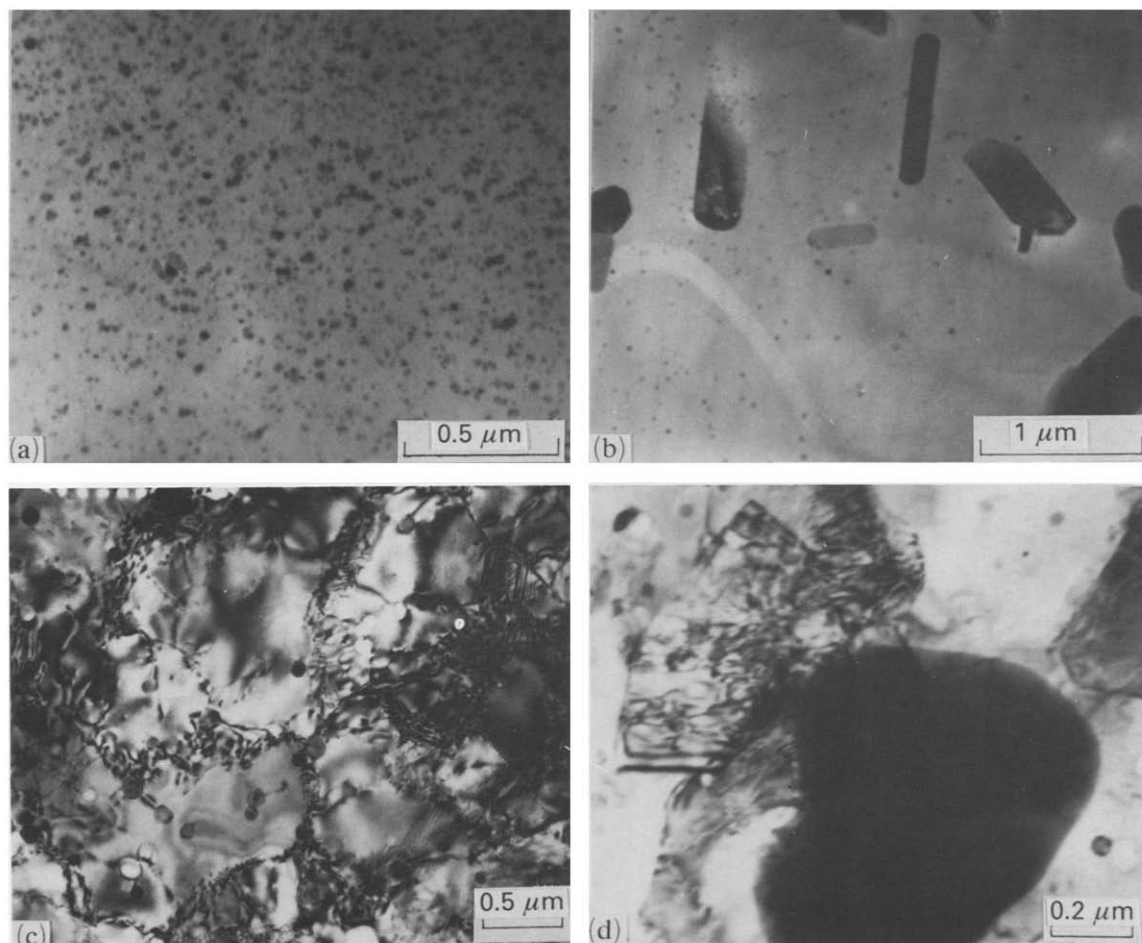


Fig. 2. Transmission electron micrographs of 7050 aluminum alloy at different steps of TMT to obtain the R microstructure: (a), (b) bright field θ and T equilibrium precipitates, respectively, taken before ageing at 400 °C for 8 h; (c) deformation structure with 85% thickness reduction at 250 °C; (d) deformation zones near the larger particles.

tion process, as shown by Humphreys [10, 15, 16].

The TMT shown schematically in Fig. 1(b) was used to obtain an unrecrystallized microstructure (UR) in the 7050 aluminum alloy. This TMT includes an initial solution heat treatment to produce a fine precipitate distribution during the rolling working operation to prevent growth of recrystallization nuclei at large inclusions, as shown by Nes [21]. The subsequent solution treatment using a low heating rate enhances the tendency towards recovery of the microstructure.

The dislocation substructure formed by an 87% reduction in thickness at 400 °C showed a more uniform distribution of dislocations, which exhibited a few defined cell walls with tangles of high dislocation density inside the cells (Fig. 3(a)). In this case, the dislocation motion to the cell

walls might have been obstructed by fine particles precipitated during quenching and/or worked operation. In the solution-treated condition the microstructure showed two distinct regions: (a) 76% of the microstructure was formed by unrecrystallized grains containing subgrains; and (b) 24% was formed by unrecrystallized grains without subgrains (Fig. 3(b)).

The subgrains are formed by a process in which the dislocation substructure progresses towards a lower energy state. The substructural rearrangement proceeds by the annihilation of the nearest redundant dislocations in cell walls and the rearrangement of the walls into more orderly arrays [19–23]. The walls become sharper and the interior dislocations are attracted into them; consequently the cells polygonize into subgrains. The unrecrystallized grains without

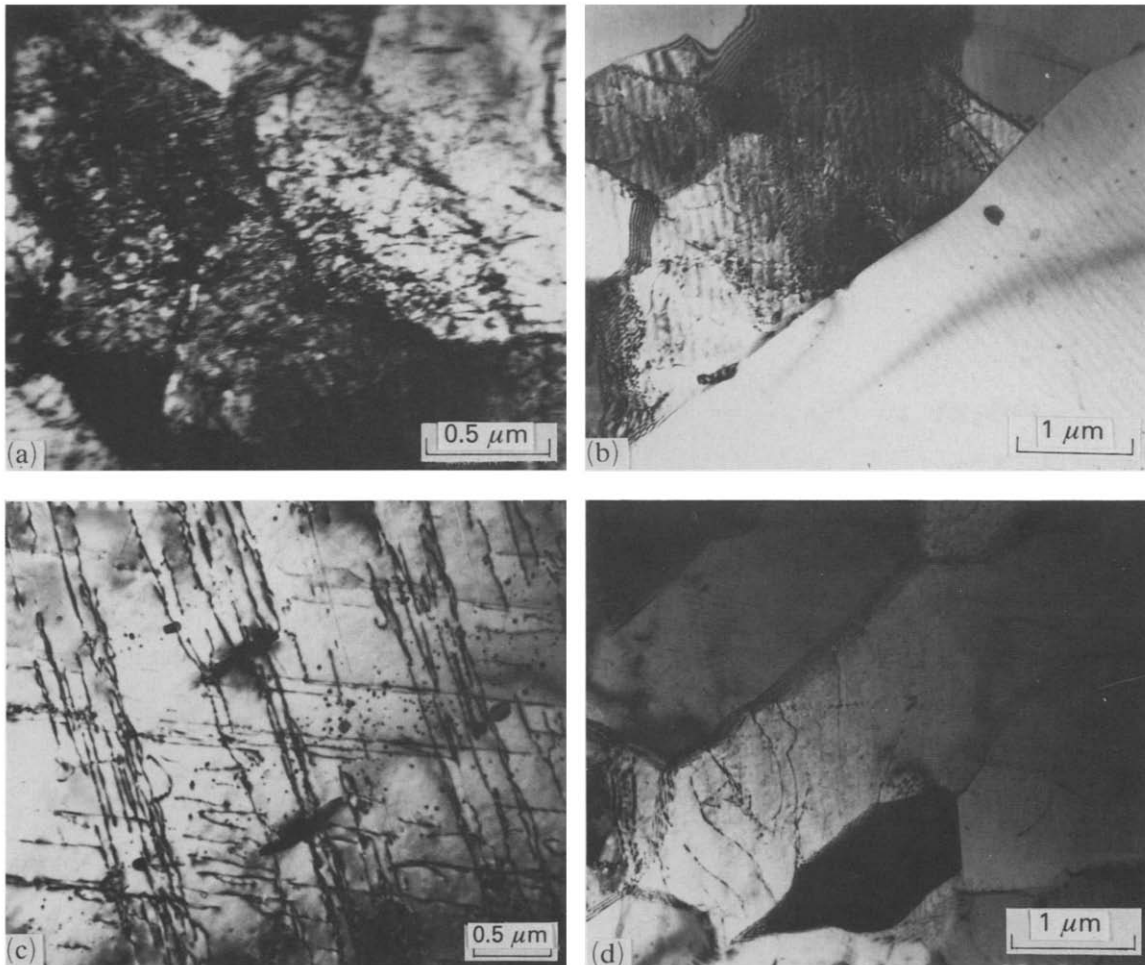


Fig. 3. Transmission electron micrographs of 7050 aluminum alloy at different steps of TMT to obtain UR microstructures: (a) deformation structure before an 87% thickness reduction by rolling; (b) duplex regions before subsequent solution treatment at 480 °C for 30 min; (c) after solution treatment showing the deformation structure in region.

subgrains show a planar dislocation substructure as seen in Fig. 3(c). However, the nature of the restoration process in the latter regions remains uncertain in this paper. The high density of dislocations suggests that it is unlikely that saturation recrystallization *in situ* around the inclusions has occurred.

The results of quantitative measurements of the microstructural parameters are given in Table 1 and the optical and electron micrographs are shown in Fig. 4 for the PR (as-received material), R and UR microstructures.

3.2. Mechanical behavior

3.2.1. Monotonic tensile parameters

The tensile properties associated with R and UR microstructures in the T76 condition are summarized in Table 2 along with the properties

of 7050 T76 as-received material with the PR microstructure for comparison. Four samples were tested for each microstructural condition and no significant variation between them was observed. The experimental results showed that the monotonic tensile properties for the materials processed by TMT had only a small improvement over the as-received material and no significant difference between monotonic tensile properties for the R and UR microstructures was observed.

The higher yield strength and ductility properties presented by R and UR microstructures can be attributed to the smaller grain size produced by TMT. A grain size effect has normally been observed in age-hardened aluminum alloy when the strengthening precipitates are sheared by dislocations [4, 11, 24]. The non-uniform precipita-

TABLE 1

Microstructural parameters of 7050 T76 aluminum alloy with PR, R and UR microstructures

Alloy	Feature	Parameter	Value for various directions		
			L	S	T
PR	Grain	Size (μm)	30–300	30–90	20–300
	Subgrain	Size D (μm)	3–15	—	—
		d (μm)	—	7.6, 3.0	5.5, 2.4
	Inclusions	f_v (%)	—	1.2	0.4
		λ (μm)	—	336	65
	Precipitates	d_p (μm)	G: 19	SG: 25	SGB: 55
		f_v (%)	G: 1	SG: 1.5	SGB: 20
(μm)		G: 163	SG: 187	SGB: 105	
R	Grain	Size (μm)	20	16	17
	Inclusions	d (μm)	—	4.3, 1.7	3.5, 1.4
		f_v (%)	—	0.40	0.36
		λ (μm)	—	54.1	46.8
	Precipitates	d_p (μm)	G: 20	GB: 113	—
		f_v (%)	G: 1.5	GB: 15	—
		(μm)	G: 150	GB: 27	—
UR	Grain	Size (μm)	> 1500	20–40	100–1000
	Subgrain	Size D (μm)	1–9	—	—
		d (μm)	—	5.1, 2.1	3.6, 1.1
	Inclusions	f_v (%)	—	0.56	0.48
		λ (μm)	—	54	41
	Precipitates	d_p (μm)	SG: 28	SGB: 65	—
		f_v (%)	SG: 2.1	SGB: 23.7	—
(μm)		SG: 174	SGB: 123	—	

G, grain; SG, subgrain; SGB, subgrain boundary.

tion in the UR microstructure produces relatively soft regions inside the subgrains, consequently decreasing the strength when compared with more uniform precipitation as obtained in the recrystallized grains [19, 23] (Figs. 4(e), 4(h) and 4(i), and Table 1).

3.2.2. Fracture toughness properties

The fracture toughness properties associated with PR, R and UR microstructures are summarized in Table 3. The results were the average of five values for each condition (microstructure and direction (L–T and T–L)). The UR microstructure clearly shows significant improvement over the R microstructure. Macroscopically the decrease in fracture toughness can be associated with crack propagation by the “pop in” mechanism in the PR and R microstructures, which increased with the tendency towards a recrystallized microstructure. Figure 5 presents the characteristic load P_c vs. COD curves obtained by fracture toughness (COD) tests, showing the difference when crack propagation occurs in the overload fracture region. The essential feature is that the R microstructure exhibits higher instability in the crack propagation mode (“pop

in”). The greater difference between fracture toughness in the L–T and T–L directions for the UR microstructure can probably be attributed to the higher texture in this material.

3.3. Fracture surface and slip behavior

3.3.1. Tensile test samples

On a macroscopic scale the tensile samples showed no significant difference in fracture surface appearance in the UR, PR and R microstructures. All of them exhibited a fracture surface inclined with respect to the stress axis, evidently following a plane of maximum shear stress. However, microscopic observation has shown different fracture mechanisms for the R and UR microstructures.

In the UR microstructure the fracture mechanism was almost completely transgranular, showing the alternate areas containing dimples in a plane normal to the stress axis and shear areas oriented parallel to the stress axis (Fig. 6(a)). SEM and TEM studies indicated that the transgranular fracture is nucleated by a concentration of shear in slip bands due to planar localized slip, which develops when coherent and/or semicoherent precipitates are sheared by dislocations [2, 12].

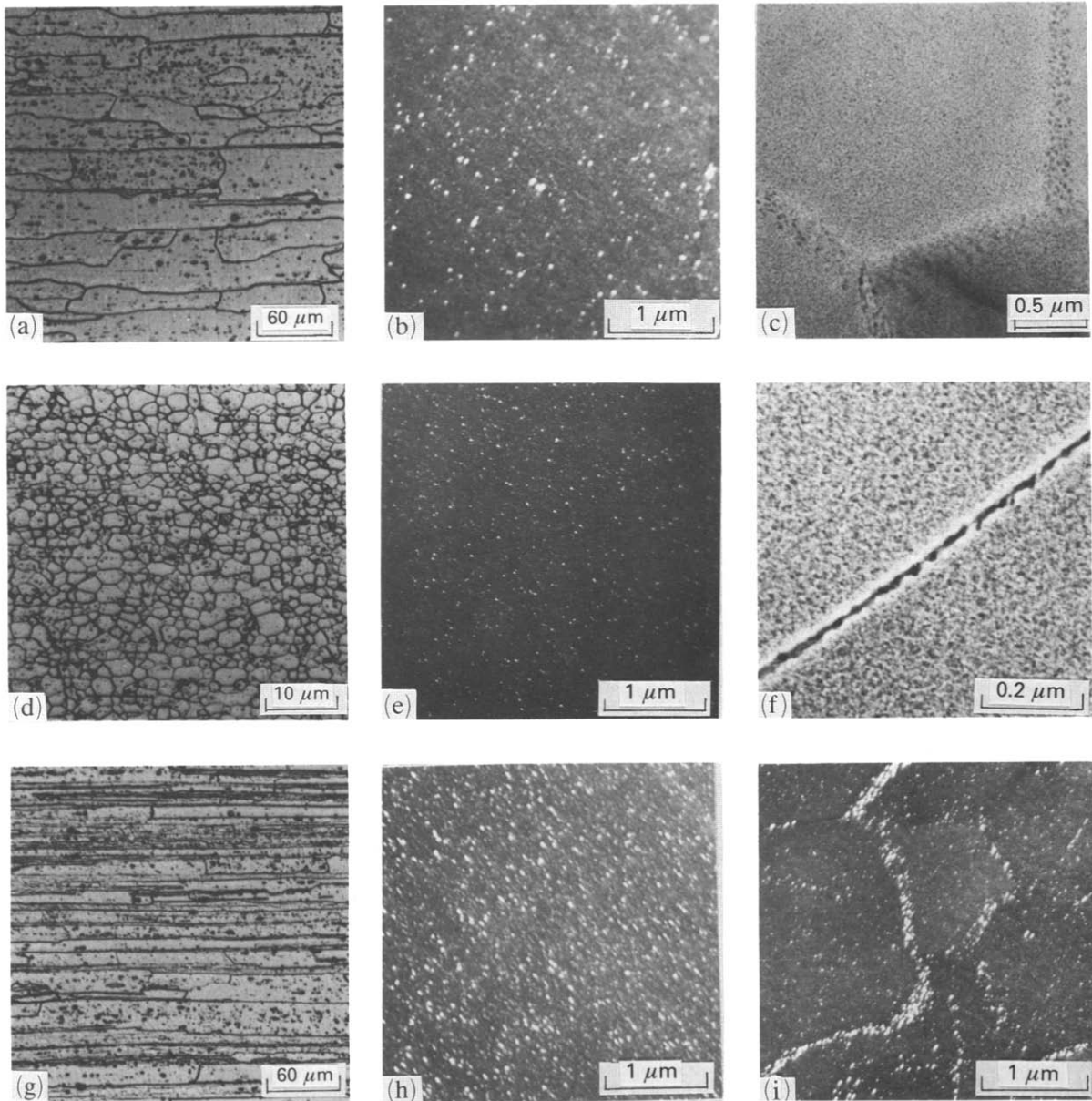


Fig. 4. Optical and transmission electron micrographs: (a) PR optical microstructure; (b), (c) hardened precipitate distribution inside the grain and subgrain, respectively, in the PR microstructure; (d) R optical microstructure; (e), (f) hardened precipitate distribution inside the grain and grain boundary, respectively, in the R microstructure; (g) UR optical microstructure; (h), (i) hardened precipitate distribution inside the subgrain and in the subgrain boundary, respectively, in the UR microstructure.

TABLE 2

Monotonic tensile properties of 7050 T76 aluminum alloy with PR, R and UR microstructures

Alloy	$\sigma_{0.2}$ (MPa)	σ_{uts} (MPa)	Elongation (%)
PR	515	549	10
R	552	575	15
UR	540	570	17

The appearance of shearing areas suggests that the shearing concentration occurs in grain boundary triple junctions, which can be originated by grain boundary sliding. Dahmen and Hornbogen [25] and Sanders and Starke [8] have shown that grain boundary sliding in aluminum-base alloys can take place at room temperature. The slip lines in the electron micrographs of Fig. 6(b) suggest that

TABLE 3

Fracture toughness COD of 7050 T76 aluminum alloy with PR, R and UR microstructures

Alloy	Direction	a (mm)	Y	P (N)	V_p (mm)	K (MPa m ^{1/2})	P_c (N)	CTOD (mm)
PR	L-T	4.86	7.61	980	1.27	25.1	34.3	0.50
	T-L	4.31	8.63	767	0.64	22.1	34.3	0.23
R	L-T	4.63	7.95	847	0.57	22.4	94.1	0.22
	T-L	4.52	7.68	870	0.40	22.3	102	0.16
UR	L-T	4.54	8.0	1020	3.74	27.2	0	1.39
	T-L	4.82	8.10	986	2.04	26.6	0	0.62

a , size of fatigue crack; $Y=f(a/w)$ where w is the width of sample; P , load; V_p , displacement; K , stress intensity factor; P_c , load difference corresponding to "pop-in"; CTOD, fracture toughness.

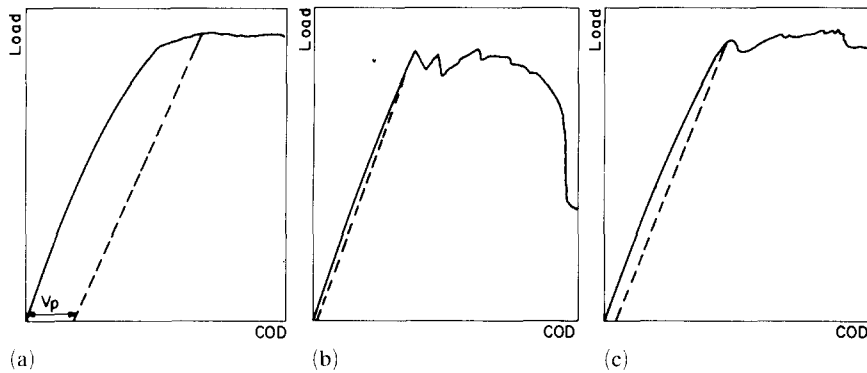


Fig. 5. Load P_c vs. COD characteristic curves obtained in COD tests for (a) the PR microstructure, (b) the R microstructure and (c) the UR microstructure.

the slip is compatible with the adjacent grain. If grain boundary sliding can occur on only one boundary comprising a triple junction the crack will form at the junction [8]. Once the crack has been nucleated the strain is concentrated in the crack tip, locally intensifying the stress. The crack propagates transgranularly along the intense slip band and accelerates the linkage of voids which have been nucleated at coarse particles and dispersoids.

The recrystallized microstructure showed a predominantly intergranular fracture surface, although some transgranular areas are evident (Fig. 7(a)). The microstructure R also showed planar slip, but with coarser slip bands and a clear tendency towards strain localization in grain boundaries (Fig. 7(b)). These slip bands, which finish on a grain boundary, produce a strain concentration on the primary slip plane owing to the work softening effect when the precipitates are sheared by the motion of dislocations [2, 4, 24]. Owing to the restriction of slip, which results from the difficulties of transferring plasticity from a favorably oriented grain to a less favorably

oriented adjacent grain, the dislocations impinge upon the grain boundary and cause a stress concentration across the boundary [1, 4, 10, 26]. This can be seen in the electron micrographs taken during *in situ* deformation studies by TEM (see Fig. 9 below). Then the nucleation of voids in non-deformable grain boundary precipitates is easier than initiating slip in a less favorably oriented grain. Once the voids are nucleated, the process of growth and coalescence occurs quite easily, owing to the concentration of strain in precipitate-free zones [4, 26, 27].

3.3.2. COD test samples

SEM surface observations on the overload region of the samples submitted to COD tests showed a similar fracture surface to that of the samples submitted to tension tests. Consequently we can connect the presence of "pop in" instability with an intergranular fracture surface such as in the case of the R microstructure. We can also establish a relationship between the size of the stretched zone, which represents the blunting of the crack tip before fracture due to overload

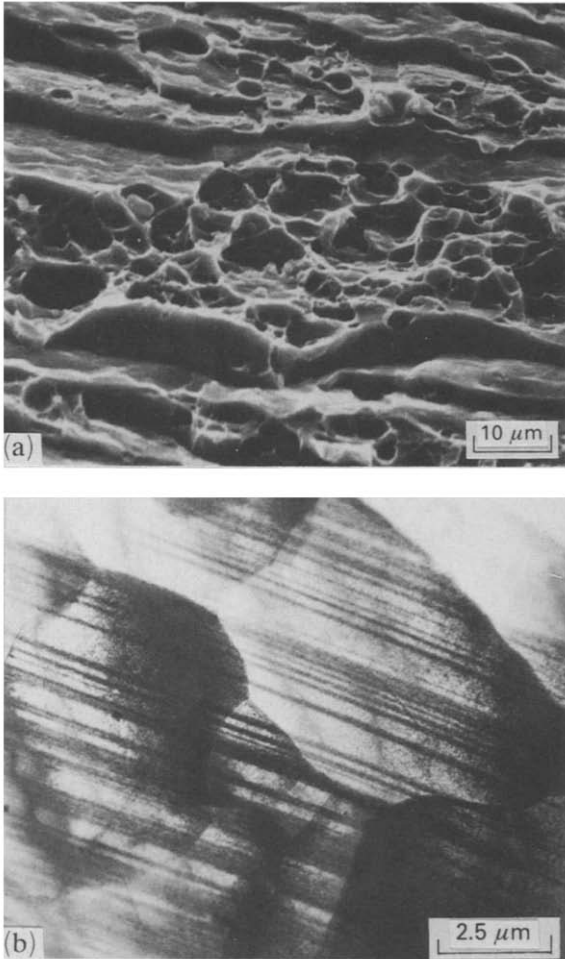


Fig. 6. (a) Scanning electron micrograph taken on the fracture surface of UR microstructure tensile samples showing a transgranular fracture surface containing alternate dimples plus shear areas; (b) transmission electron micrograph taken from tensile samples strengthened at 2% elongation showing slip line behavior.

[28–30], with the fracture toughness. The scanning electron micrographs shown in Fig. 8 are characteristic of the typical morphology presented by the stretched zone. It is assumed that they correspond to the fatigue crack tip regions where the crack extends throughout the plastic zone at the onset of fast overload fracture. The individual and average values of the size of the stretched zone associated with the R and UR microstructures are presented in Table 4. These values are proportional to CTOD at the onset of fast overload fracture [28, 30], *i.e.* $CTOD_i = 2d$, where d is the size of the stretched zone. The values of $CTOD_i$ calculated using Table 4 showed the same tendency with respect to fracture toughness as was obtained previously from the COD

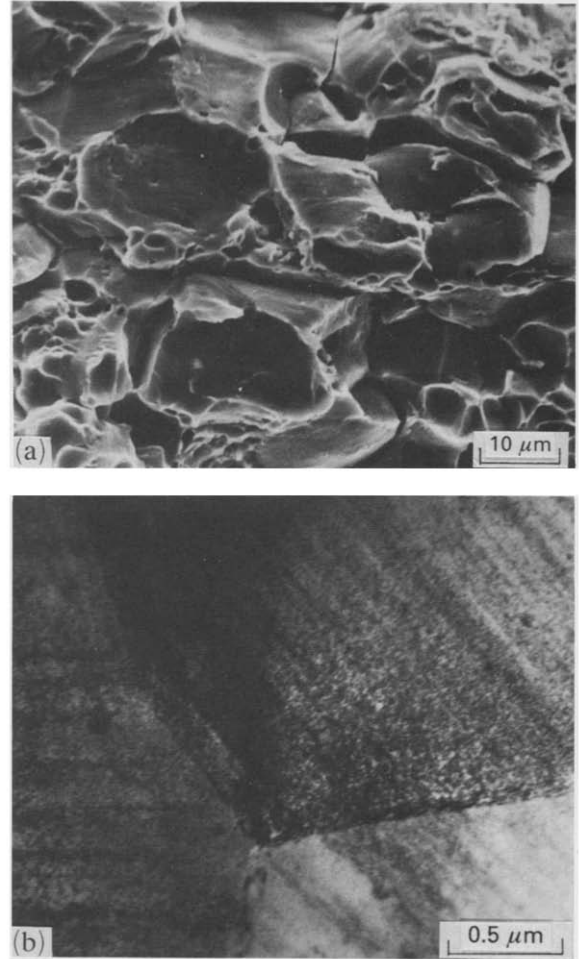


Fig. 7. (a) Scanning electron micrograph taken on the fracture surface of R microstructure tensile samples showing an intergranular fracture surface; (b) transmission electron micrograph taken from tensile samples strengthened at 2% elongation showing slip line behavior.

tests. The values of fracture toughness obtained from the stretched zone height are obviously smaller than those obtained from the COD tests, since they represent the onset of fracture and the “pop in” effect is not considered, consequently decreasing the difference in fracture toughness between the R and UR microstructures.

Considering the hypothesis that the plastic zone at the crack tip can reasonably be represented as made up of “overlapping regions of shear” [1, 31, 32], it follows that the strain distribution inside the plastic zone is not homogeneous, but concentrates in slip bands of maximum shear stress. This hypothesis was confirmed by TEM during *in situ* deformation studies of thin foil (Figs. 9(a) and 9(b)). The fracture process in the UR microstructure suggests that the crack

propagation is due to a strain concentration effect at the crack tip, generating slip along the planes of maximum shear stress. Consequently the crack opens through the new surfaces generated by dislocation movement, and at the same time extends in length [28, 33–36]. Increasing stress and strain

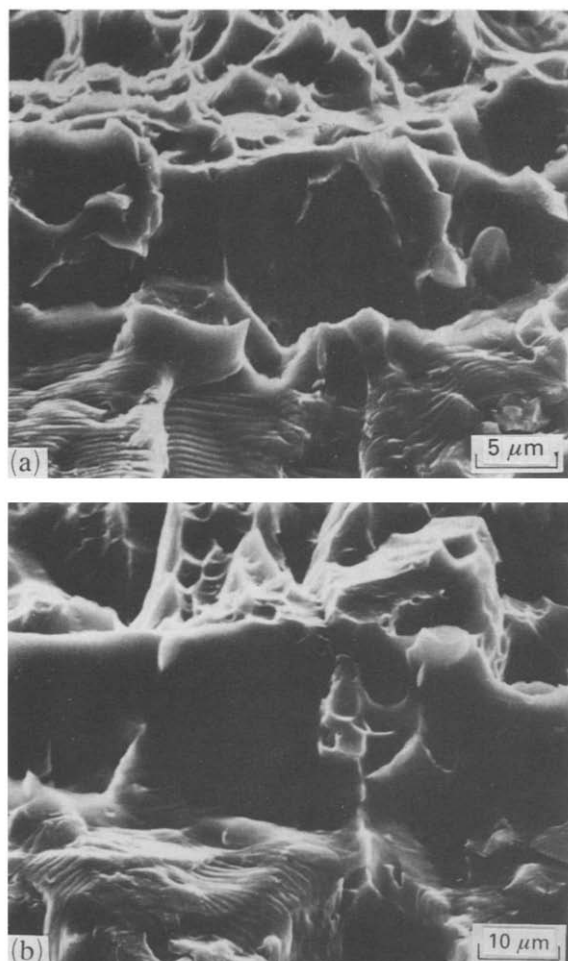


Fig. 8. Scanning electron micrographs taken on the fracture surface of COD samples showing details of the transition region between the fatigue zone and the overload zone: (a) R microstructure; (b) UR microstructure.

will activate other parallel slip planes and gradually lead to blunting of the crack tip. This process produces a lateral increase in size of the plastic zone until the deformation level in the slip bands reaches a critical value for void coalescence due to void growth inside these bands, which were nucleated around the inclusions and dispersoids. Hard precipitates can accelerate the fracture process, since they assist the strain concentration in bands of maximum slip [2, 11].

In the R microstructure, slip bands generated along the planes of maximum shear stress, inside the plastic zone, lead to less blunting of the crack tip. In this case the strain concentration occurs preferentially in grain boundaries, owing to the difficulty of transferring plasticity from favorably oriented grains to less favorably oriented adjacent grains (Fig. 9(c)). The stress concentration required for the coalescence of voids at grain boundary precipitates was greater than that necessary for the coalescence of voids at the particles (inclusions and dispersoids) inside the matrix, since the fracture propagated intergranularly. Thus the volumetric fraction of precipitates in the grain boundary, the precipitate-free zones (which were present in the R microstructure (Fig. 4(f)) and the grain size (which is proportional to the pile-up length) must be the more important parameters for controlling the fracture toughness in R microstructures.

4. Conclusions

The recovery process in the UR microstructure is assisted by the distribution of fine precipitates, which produces a homogeneous strain distribution during work operation and consequently hinders the motion of dislocations during solution heat treatment. Otherwise the recrystallization mechanism in the R microstructure is dependent on the strain concentration at coarse particles.

TABLE 4

Stretched zone dimensions obtained in COD test samples for the PR, R and UR microstructures

Alloy	Stretched zone (μm)			
	L-T		T-L	
	Individual values	Average	Individual values	Average
PR	24.1, 12.7, 19.0, 17.8	18.4	17.8, 6.3, 6.5, 19.0, 17.8	13.5
R	16.0, 15.8, 12.6, 19.0, 16.5, 9.0	16.5	15.6, 12.7, 16.2, 12.1	14.2
UR	31.7, 25.4, 30.4, 34.2, 26.6	30.1	17.8, 12.7, 27.4, 15.3	18.3

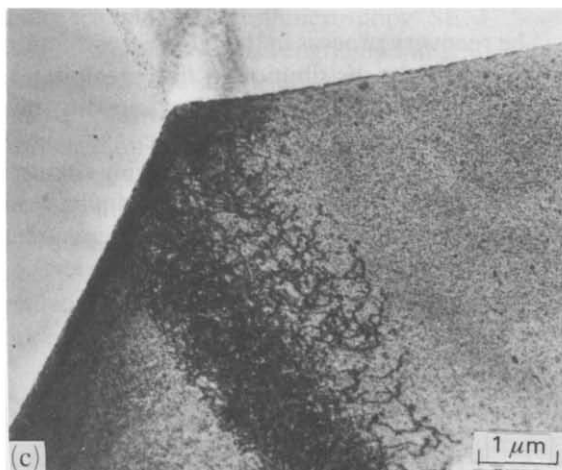
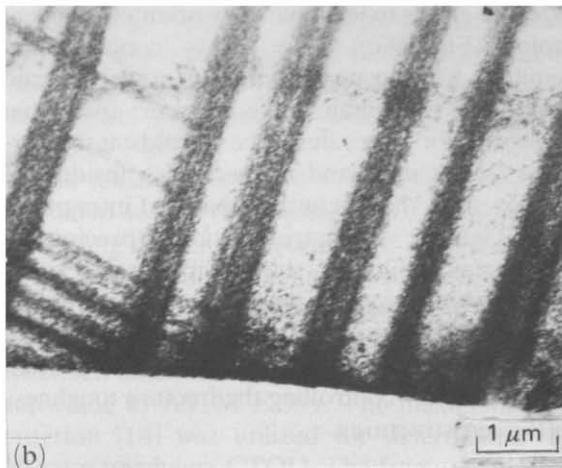
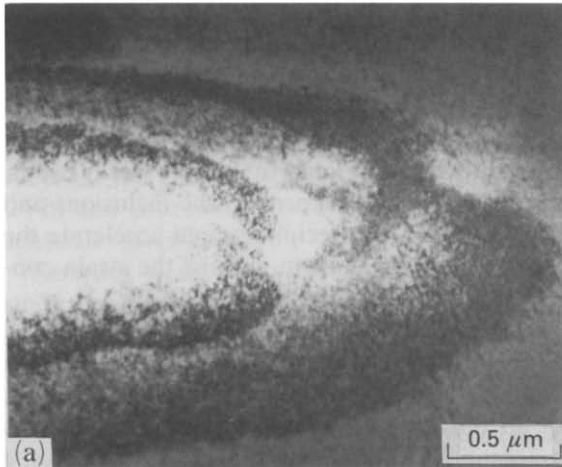


Fig. 9. Transmission electron micrographs taken during *in situ* deformation studies: (a) UR microstructure, plastic zone around the crack tip; (b) UR microstructure, slip bands of maximum shear stress inside the plastic zone obtained on the crack flank before fracture; (c) R microstructure, dislocation impingement upon the grain boundary and stress concentration.

The UR microstructure shows only a small improvement in monotonic tensile properties over the PR and R microstructures, but a drastic improvement in fracture toughness was observed in the UR microstructure. The increase in fracture toughness is due to a crack propagation transition mode with a change from predominantly transgranular propagation in the UR microstructure to a mixed mode in the PR microstructure and predominantly intergranular propagation in the R microstructure. Both PR and R microstructures show “pop in” instability during crack propagation.

The crack propagation in the IR microstructure is due to a strain concentration effect at the crack tip, generating slip bands along the planes of maximum shear stress and producing nucleation, growth and coalescence of voids inside these slip bands. Otherwise, the R microstructure has a clear tendency towards strain localization in grain boundaries; consequently the nucleation and coalescence of voids at non-deformable precipitates in grain boundaries is easier than the initiation of slip in a less favorably oriented adjacent grain.

Acknowledgment

The authors would like to acknowledge Professor Arno Blass for reviewing the English text.

References

- 1 G. T. Hans and A. R. Rosenfield, *Metall. Trans.*, 6 (1975) 653.
- 2 E. Hornbogen and K.-H. Zum Garh, *Metallography*, 8 (1975) 181.
- 3 A. R. Rosenfield, *Met. Rev.*, 121 (1968) 29.
- 4 E. A. Starke, Jr. and F. S. Lin, *Metall. Trans.*, 13 (1982) 2259.
- 5 B. K. Park and J. E. Vrugink, in T. G. Moris (ed.), *Thermomechanical Processing of Aluminum Alloys*, AIME, Warrendale, PA, 1979, p. 25.
- 6 E. Di Russo, M. Conserva, M. Buratti and F. Gatto, *Mater. Sci. Eng.*, 14 (1974) 23.
- 7 E. Di Russo, M. Conserva, F. Gatto and H. Markus, *Metall. Trans.*, 4 (1973) 1134.
- 8 T. H. Sanders and E. A. Starke, Jr., *Acta Metall.*, 30 (1982) 927.
- 9 D. Broek, *Elementary Engineering Fracture Mechanics*, Martinus Nijhoff, The Netherlands, 1984.
- 10 O. E. Alarcon, Influencia do TMT na microestrutura, no comportamento mecanico e no mecanismo de fratura da liga de aluminio 7050 T76, *Dr. Tesis*, Departamento de Engenharia de Materiais, Faculdade de Engenharia de Campinas/Universidade Estadual de Campinas, 1988. Campinas.

- 11 L. N. Mueller, ALCOA aluminum alloy 7050, *Green Letter 220*, 2nd revised edn., ALCOA Center, Pennsylvania, November 1983.
- 12 J. W. Martin, *Micromechanisms in Particle-Hardened Alloys*, Pergamon, Oxford, 1980, Chapter 2, p. 85.
- 13 E. D. Underwood, in McCall and Steele (eds.), *Practical Applications of Quantitative Metallography*, *Am. Soc. Test. Mater., Spec. Tech. Publ.*, 1982, p. 839.
- 14 British Standard Methods for Crack Opening Displacement (COD) Testing, *BS 5762*, 1979.
- 15 F. J. Humphreys, *Acta Metall.*, 25 (1977) 1323.
- 16 O. E. Alarcon and A. M. M. Nazar, *Proc. 8 Congresso Brasileiro de Engenharia e Ciencia dos Materiais—CBECIMAT, Campinas*, Mecanismos de Recristalização em Liga de Alumínio 7050, 1988, p. 132.
- 17 J. A. Wert, N. E. Paton, C. H. Hamilton and M. W. Nohoney, *Metall. Trans.*, 12 (1981) 1267.
- 18 J. D. Embury and R. B. Nicholson, *Acta Metall.*, 13 (1965) 403.
- 19 H. J. McQueen, *Metall. Trans.*, 8 (1977) 807.
- 20 A. W. Thompson, *Metall. Trans.*, 8 (1977) 833.
- 21 E. Nes, *Acta Metall.*, 24 (1976) 391.
- 22 P. G. Shewmon, *Transformations in Metals*, McGraw-Hill, New York, 1969, Chapter 3, p. 205.
- 23 H. J. McQueen, in T. G. Morris (ed.), *Thermomechanical Treatment of Aluminum Alloys*, AIME, Warrendale, PA, 1974, p. 1.
- 24 E. Hornbogen, *Proc. 6th Int. Conf. on the Strength of Metals and Alloys*, Vol. 3, Gifkins, Melbourne, 1982, p. 1059.
- 25 U. Dahmen and E. Hornbogen, *Z. Metallkd.*, 6 (1974) 901.
- 26 A. K. Vasudevan and R. D. Doherty, *Acta Metall.*, 35 (6) (1987) 1193.
- 27 N. Rium, *Acta Metall.*, 17 (1969) 921.
- 28 D. Broek, *Eng. Fract. Mech.*, 6 (1974) 173.
- 29 J. D. Harrison, *Met. Constr.*, 10 (1980) 524.
- 30 R. C. Bates, *Electron Micrography*, *Am. Soc. Test. Mater., Spec. Tech. Publ.*, 543 (1969) 192.
- 31 G. G. Garret and J. F. Knott, *Metall. Trans.*, 9 (1978) 1187.
- 32 C. G. Chen and J. F. Knott, *Met. Sci.*, 15 (1981) 357.
- 33 E. Di Russo, *Metall. Sci. Technol.*, 4 (2) (1986) 37.
- 34 S. M. Ohr, *Mater. Sci. Eng.*, 72 (1985) 1.
- 35 H. G. F. Wilsdorf, *Mater. Sci. Eng.*, 59 (1983) 1.
- 36 O. E. Alarcon, W. A. Monteiro and A. M. M. Nazar, *Proc. IX Inter-American Conf. on Materials and Technology*, Santiago, 1987, p. 291.